Synthesis, characterization and stability properties of Cl-bearing hydrotalcite-pyroaurite solids

By K. Rozov*, H. Curtius, A. Neumann and D. Bosbach

Forschungszentrum Jülich, Institut für Energie- und Klimaforschung (IEK-6), 52425 Jülich, Germany

Summary. A layered double hydroxides (LDH) hydrotalcite-pyroaurite solid solution series $(Mg_{1-x}Fe(II)_x)_3Al_1Cl_1 \cdot nH_2O$ with variable $x Fe_{solid} = Fe^{2+}/(Fe^{2+} + Mg^{2+})$ iron mole fractions were studied in co-precipitation experiments at $T = 25$, 40, 45, 50, 55 and 60 °C and pH $= 10.00 \pm 0.05$. The compositions of the solids and reaction solutions were determined using ICP-OES, EDX (Mg, Al, Fe) and TGA techniques (Cl^-, OH^-, H_2O). Powder X-ray diffraction was applied for phase identification and determination of unit-cell parameters $a_o = b_o$ and c_o from Bragg evaluation. Syntheses products containing $x Fe_{solid} > 0.13$ display additional X-ray patterns attributed to the mixture of iron oxides and hydroxides. On the other side, precipitates with $0 \leq x Fe_{solid} \leq 0.13$ show only X-ray reflexes typical for pure LDH compositions. Moreover, in this case unit-cell parameters $a_o = b_o$ as a function of $x Fe_{solid}$ follow Vegard's law corroborating the existence of a continuous solid solution series. TGA data demonstrated the temperatures at which interlayer H_2O molecules and Cl^--anions are lost, and at which temperatures dehydroxylation of brucite-like layer occurs. Based on detailed analyses of TGA curves it was established that the increase of $x Fe_{solid}$ does not result in a visible change of the thermal stability of hydrotalcite-pyroaurite solids. From the chemical analyses of both the solids and the reaction solutions after syntheses, preliminary Gibbs free energies of formation were estimated by using GEMS-PSI code package. Values of G_f°(Hydrotalcite) $= -3619.04 \pm 15.27$ kJ/mol and G_f°(Pyroaurite) $= -2703.61 \pm 191.93$ kJ/mol were found at 298.15 K. A comparison of our estimate with G_f° value -3746.90 ± 11.00 kJ/mol for CO_3^{2-}-bearing hydrotalcite presented in our previous studies, denotes the effect of intercalated anion on the aqueous solubilities of LDH when Cl-containing solids have to be more soluble than CO_3^{2-}-bearing substances. Estimation of the standard molar entropy of the hydrotalcite end-member by applying Helgeson's methods and using results of co-precipitation experiments at variable temperatures let us to conclude that derivation of more precise S_f° values would require calorimetric measurements.

---

*Author for correspondence (E-mail: K.Rozov@fz-juelich.de).

1. Introduction

The disposal of radioactive waste (especially, spent fuel elements) in natural geological environments calls for the development of new radionuclide-binding materials. These materials have to: (1) be physically and chemically stable at repository conditions for a long enough time to ensure that radioactive decay will greatly reduce the level of activity and (2) prevent the migration of different (*i.e.*, cationic and anionic) radioactive compounds and their decay products from deep geological conditions to the biosphere. Layered double hydroxide phases (LDHs) or hydrotalcite-like solids are of interest to these studies due to their ability to retain very wide range of different cations (like, Li^+, Ba^{2+}, Mg^{2+}, Fe^{2+}, Ni^{2+}, Al^{3+}, Fe^{3+}, Cr^{3+}, Ga^{3+}, Sc^{3+}, Zr^{4+}, *etc.*) [1–7] and especially due to their anion-exchange properties (substitutions of I^-, Br^-, Cl^-, OH^-, CO_3^{2-}, SO_4^{2-}, $Fe(CN)_6^{4-}$, carboxylates, sulfonates or dicarboxylates $C_nH_{2n}(CO_2^-)_2$, *etc.*) [8–15]. The anion-exchange properties of LDHs with general formula $[M^{II}_{(1-x)}M^{III}_{(x)}(OH)_2]^{x+}[A^y_{x/y} \cdot nH_2O]^{x-}$ result directly from their structure which is composed of positively charged brucite-like layers (the first set brackets) and intercalated anions which are accompanied by molecules of water (the second set of brackets in the formula). This means that LDHs can be considered especially as potential buffer materials in multibarrier systems for retention of mobile, soluble and long-lived radioactive anions (like, ^{14}C, ^{129}I, ^{36}Cl, ^{79}Se *etc.*) [16]. However, the understanding of the retention properties, behavior of LDHs in aqueous environment and finally, applying these substances for geochemical modeling at conditions of nuclear repositories are hampered by scarce information on their thermodynamic and solubility properties. The problem of retrieving thermodynamic data and predicting stability of LDHs have been recently touched only in a few studies [8, 17–20]. This work on the synthesis, characterization of a particular case of big LDH family, namely, chloride-bearing hydrotalcite (Htlc) $Mg_3Al(OH)_8Cl \cdot nH_2O$ – pyroaurite (Pyr) $Fe(II)_3Al(OH)_8Cl \cdot nH_2O$ solids because they have been identified as characteristic secondary phase components in corrosion products under repository conditions of disposed nuclear fuel elements [4, 21]. Using various experimental techniques (X-ray powder diffraction, infrared spectroscopic measurements, thermogravimetric
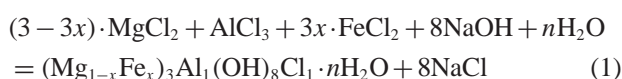
analysis, scanning electron microscopy, energy dispersive X-ray spectroscopy), the primary objective was to ascertain the presence of a continuous solid solution series between hydrotalcite and pyroaurite (*i.e.*, isostructural substitution of Mg by Fe(II)). The next objectives were to quantify the standard Gibbs free energies and entropies of formation with the help of thermodynamic modeling [22] based on the chemical analysis of solid and liquid phases at equilibrium and to provide temperature corrections for thermodynamic properties of solids by using data from synthesis experiments at different (25, 40, 45, 50, 55 and 60 °C) temperatures.

2. Materials and methods

2.1 LDH synthesis

Samples of hydrotalcite-pyroaurite solids with varying mole fractions of iron(II) $x\text{Fe}_{\text{solid}} = \text{Fe}^{2+}/(\text{Fe}^{2+} + \text{Mg}^{2+})$ were synthesized by a co-precipitation method at $T = 25, 40, 45, 50, 55$ and 60 °C and pH $= 10.00 \pm 0.05$. The syntheses were performed under argon gas flow by slow addition (at a rate 0.2–0.3 mL/min) of 50 mL degassed metal-chloride solution with $(\text{Mg}^{2+} + \text{Fe}^{2+})/\text{Al}^{3+} = 3.0 \pm 0.1$ into a reactor vessel containing 350 mL of boiled MilliQ water under stirring. To maintain pH $= 10.00 \pm 0.05$, 2 M NaOH solution was added simultaneously into the reactor using an automated titrator 736 GP TITRINO. The overall reaction of synthesis can be described as:

$$(3 - 3x) \cdot \text{MgCl}_2 + \text{AlCl}_3 + 3x \cdot \text{FeCl}_2 + 8\text{NaOH} + n\text{H}_2\text{O}$$
$$= (\text{Mg}_{1-x}\text{Fe}_x)_3\text{Al}_1(\text{OH})_8\text{Cl}_1 \cdot n\text{H}_2\text{O} + 8\text{NaCl} \qquad (1)$$

After the addition step, the stirring was continued for 24 h under controlled pH (pH $= 10.00 \pm 0.05$) and needed temperature. The precipitate and supernatant liquid were then separated by using 0.22 µm MILLEX® GP filters. The formed solid was washed three times by boiled MilliQ water and dried in a desiccator for 72 h.

2.2 Chemical analyses of solid and liquid phases

2.2.1 ICP-OES analyses

The contents of Mg, Fe, Al and Na in the solids and supernatant liquids were determined by ICP-OES method using TJA-IRIS™ instrument. The supernatant solutions were analyzed after acidifying with drops of 8 M HNO₃. The solid samples were analyzed after dissolving in 2 M HNO₃. Solutions of internal standards were prepared from MgCl₂·6H₂O, FeCl₂·4H₂O, AlCl₃·6H₂O and NaCl chemicals (Merck®).

2.2.2 Photometric analyses

Chloride anions in the product liquid phase and in synthesized solids were analyzed photometrically (spectrophotometer CADAS 100). The solid samples were analyzed after dissolving in 2 M HNO₃. The supernatant liquids were measured after dilution (1 : 10 and 1 : 100) with degassed MilliQ water. Solutions of NaCl were used for the preparation of internal standards.

2.3 Powder X-ray diffraction (PXRD)

The powder X-ray diffraction measurements were applied for structural characterization of the synthesized solids with respect to long-range ordering by using a 3003 TT (General Electric) diffractometer (Bragg-Brentano geometry). No internal standards for possible specimen displacement were used. The samples were measured from 5 to 85° 2Θ with a step size of 0.02° 2Θ and a measuring time of 15 s per step. The cell parameters were calculated from the Bragg equation and using relation between indexed d_{hkl} distances and the lattice unit-cell parameters for hexagonal symmetry based on the first 4 reflections: (003), (006), (012), and (015).

2.4 Infrared spectroscopy

Infrared spectra of precipitates were acquired using an FTIR Bruker Equinox spectrometer in order to identify the interlayer composition (anions and water-molecules). Pellet samples were prepared by weighing approximately 200 mg KBr powder (Merck®) together with approximately 2 mg of each sample (1% by mass) which were finally mixed and pressed in 20 mm disks. Spectra were recorded in the wavenumber interval from 800 to 4000 cm⁻¹.

2.5 Thermogravimetric analyses (TGA)

TGA-DSC was carried out in order to determine the contents of interlayer water, hydroxyl groups and chloride-anions in solids. Measurements were performed on a Netzsch STA 449 C Jupiter™ instrument. The weight loss of the solids was analyzed from 25 °C to 1000 °C with a heating rate of 10 °C/min, under a nitrogen flow.

2.6 Scanning electron microscopy (SEM) and energy dispersive X-ray spectroscopy (EDX)

In order to investigate the morphology of synthesized crystallites the low-pressure scanning electron microscopy (SEM) photographs were taken with a Quanta 200 microscope. Examinations were performed at a pressure of 70 Pa. Additional quantitative chemical analyses of solids (content of Mg, Fe, Al, Cl, C, O) and information about chemical homogeneity of precipitates were carried out with energy dispersive X-ray spectroscopy (EDX) an Apollo X Silicon Drift Detector from EDAX™, at a voltage of 20 kV.

3. Thermodynamic modeling

3.1 Estimation of Gibbs free energies

Gibbs free energies of formation of the solids at $T = 25, 40, 45, 50, 55$ and 60 °C were estimated under assumption of the thermodynamic equilibrium between synthesized solids and liquid phases after synthesis experiments. This assumption was used because our previous co-precipitation and long-term (> 140 day) dissolution tests with CO_3^{2-}-bearing hydrotalcites [19] had clearly shown a non-significant oversaturation degree in aqueous solutions after analogous syntheses. Therefore, in the present study the following scheme

of $G_f^\circ(298)$ estimations has been applied: 1) using results of chemical analyses the speciation of aqueous phases has been modeled in order to calculate activities and chemical potentials of all relevant components (*i.e.*, Mg^{2+}, Fe^{2+}, Al^{3+}, OH^-, Cl^-). For this purpose we used the Gibbs free energy minimization software GEM-Selektor [22] with built-in NAGRA-PSI and SUPCRT/Slop98 chemical thermodynamic database [23, 24]; 2) on the second step, we applied the statement of the thermodynamic equilibrium which says that: Gibbs free energy of the system at the equilibrium is minimum, and chemical potentials of the components at equilibrium are the same in each phase. This permitted the determination of the Gibbs free energies from chemical potentials of solutes and from the stoichiometric coefficients in Tables 3 and 4 according to:

$$G_f^\circ(\text{Htlc-Pyr}) = a\mu(Mg^{2+}) + b\mu(Fe^{2+}) + c\mu(Al^{3+})$$
$$+ d\mu(OH^-) + e\mu(Cl^-) \tag{2}$$

where $a-e$: stoichiometric coefficients; μ – chemical potentials, calculated from the supernatant liquid composition.

### 3.2 Estimation of absolute molar entropies of formation

We estimated the absolute molar entropies at 298 K and 1 bar in order to provide temperature and pressure corrections for Gibbs free energies of synthesized hydrotalcite solids. This has been done applying two different approaches: 1) the method of Helgeson [25] (see below); and 2) based on results of hydrotalcite syntheses at various temperatures (25, 40, 45, 50, 55 and 60 °C).

By applying the approach of Helgeson [25] we considered the absolute molar entropy (236.66 J/mol K) of the carbonate-bearing hydrotalcite $Mg_3Al(OH)_8(CO_3)_{0.5}$ investigated in co-precipitation and dissolution experiments at ambient (23 ± 2 °C, 1 bar) conditions [19]. Then, we constructed the hypothetical anion-exchange reaction between carbonate-containing composition and chloride-bearing solid:

$$Mg_3Al(OH)_8(CO_3)_{0.5} + Cl^-_{(aq)} \leftrightarrow$$
$$Mg_3Al(OH)_8Cl_1 + 0.5CO_3^{2-}_{(aq)} \tag{3}$$
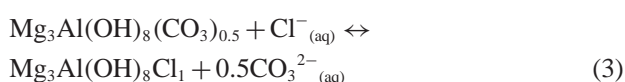
Since the reactant and product solids have similar structures, the approximation can be made (following [25]) that $\Delta_r S^\circ$ is zero. This assumption and the data on the entropies of Cl^- and CO_3^{2-} aqueous species (56.735 and -49.999 J/mol K, respectively [24]) allowed to estimate the absolute molar entropy of the chloride-bearing hydrotalcite substance.

The experimental method to evaluate the absolute molar entropy of hydrotalcite was based on the temperature dependence of the molar Gibbs free energies of synthesized hydrotalcites. In the first step, we used results of chemical analyses of hydrotalcite solids and corresponding supernatant liquids from syntheses at different temperatures (25, 40, 45, 50, 55 and 60 °C) and obtained values of Gibbs free energies of hydrotalcite according to the scheme described in Sect. 3.1. Then we constructed the reaction of hydrotalcite decomposition to simple aqueous species:

$$Mg_3Al(OH)_8Cl = 3Mg^{2+}_{(aq)} + Al^{3+}_{(aq)} + 8OH^-_{(aq)}$$
$$+ Cl^-_{(aq)}, \tag{4}$$
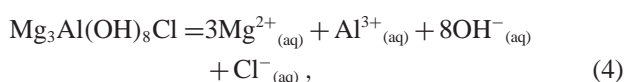
and calculated the corresponding equilibrium constants at $T = 25, 40, 45, 50, 55$ and 60 °C using free energies ($G_{f,T}$) of simple aqueous species (Mg^{2+}, Al^{3+}, OH^-, Cl^-) at given temperatures T, taken from NAGRA/PSI database [23] and using Eq. (5):

$$\Delta_r G(T) = 3G_{f,T}(Mg^{2+}_{(aq)}) + G_{f,T}(Al^{3+}_{(aq)})$$
$$+ 8G_{f,T}(OH^-_{(aq)}) + G_{f,T}(Cl^-_{(aq)}) - G_{f,T}(\text{Htlc})$$
$$= -RT \ln K \tag{5}$$

Next, we used the Van't Hoff equation (Eq. 6) in order to calculate the enthalpy effect of this reaction at 298.15 K and to find the standard enthalpy of hydrotalcite phase:

$$\ln\left(\frac{K_T}{K_{298.15}}\right) = -\frac{\Delta_r H\,(298.15\,\text{K})}{R} \times \left[\frac{1}{T} - \frac{1}{298.15}\right], \tag{6}$$

where K_T and $K_{298.15}$ – the equilibrium constants of Eq. (4) at given temperature T and 298.15 K, respectively; $\Delta_r H$ (298.15 K) – the enthalpy effect of reaction at 298.15 K. Finally, in order to calculate the entropy change in Eq. (4) and the absolute molar entropy of hydrotalcite, the fundamental relation defining the important thermodynamic functions (Gibbs free energy, entropy and enthalpy) has been applied:

$$\Delta_r S = (\Delta_r H - \Delta_r G)/T \tag{7}$$

4. Results

4.1 Compositions of solids and liquid phases after co-precipitation experiments

The compositions of liquid and solid phases after co-precipitation experiments are provided in Tables 1–4.

Table 1. Compositions of aqueous solutions (pH $= 10.00 \pm 0.05$) after hydrotalcite-pyroaurite synthesis at 25 °C.

Approximate mole fraction ($x\text{Fe}_{solid}$)	Mg	Al (μmol/kg)	Fe	Na	Cl (mmol/kg)	(Mg + Fe)/Al in aqueous phase
0.000	70.70	1.11	below DL	90.16	111.70	63.69
0.033	254.00	1.11	below DL	89.23	99.85	228.83
0.067	29.50	7.49	below DL	90.16	102.95	3.94
0.100	33.33	13.48	below DL	94.07	99.85	2.47
0.133	95.60	11.24	below DL	98.02	102.95	8.51
0.500	35.00	435.02	below DL	95.07	105.20	0.08

Table 2. Compositions of aqueous solutions (pH $= 10.00 \pm 0.05$) after hydrotalcite syntheses at 25, 40, 45, 50, 55 and 60 °C.

T (°C)	Mg	Al (μmol/kg)	Na	Cl (mmol/kg)	Mg/Al in aqueous phase
25	666.00	1.12	100.25	122.42	594.64
40	129.00	1.13	97.58	93.65	114.16
45	143.00	1.43	96.87	92.23	100.00
50	15.00	1.61	95.84	104.36	9.32
55	83.70	1.12	95.50	102.11	74.73
60	21.5	3.03	98.00	110.29	7.10

Table 3. Stoichiometric formulae of hydrotalcite-pyroaurite solids synthesized at 25 °C and pH $= 10.00 \pm 0.05$.

Mole fraction of iron in solids	Stoichiometric formulae	$(Mg^{2+}+Fe^{2+})/$ Al^{3+} in solid phase
0.000	$Mg_3Al_{1.030}(OH)_{8.187}Cl_{0.903} \cdot 2.37H_2O$	2.913
0.029	$Mg_{2.912}Fe_{0.088}Al_{1.090}(OH)_{8.490}Cl_{0.780} \cdot 2.451H_2O$	2.752
0.066	$Mg_{2.801}Fe_{0.199}Al_{1.013}(OH)_{7.723}Cl_{1.315} \cdot 3.97H_2O$	2.962
0.096	$Mg_{2.713}Fe_{0.287}Al_{1.116}(OH)_{8.731}Cl_{0.617} \cdot 2.475H_2O$	2.688
0.132	$Mg_{2.604}Fe_{0.396}Al_{0.959}(OH)_{7.696}Cl_{1.181} \cdot 2.595H_2O$	3.128

Table 4. Stoichiometric formulae of hydrotalcite solids synthesized at 25, 40, 45, 50, 55 and 60 °C and pH $= 10.00 \pm 0.05$.

T (°C)	Stoichiometric formulae	(Mg^{2+}/Al^{3+}) in solid phase
25	$Mg_3Al_{1.085}(OH)_{8.481}Cl_{0.774} \cdot 2.489H_2O$	2.765
40	$Mg_3Al_{1.017}(OH)_{8.303}Cl_{0.748} \cdot 2.309H_2O$	2.950
45	$Mg_3Al_{1.034}(OH)_{8.393}Cl_{0.709} \cdot 2.294H_2O$	2.901
50	$Mg_3Al_{1.048}(OH)_{8.626}Cl_{0.518} \cdot 2.630H_2O$	2.863
55	$Mg_3Al_{1.042}(OH)_{8.463}Cl_{0.663} \cdot 2.313H_2O$	2.879
60	$Mg_3Al_{1.047}(OH)_{8.629}Cl_{0.512} \cdot 2.367H_2O$	2.865

Tables 3 and 4 reveal the average $(Mg^{2+} + Fe^{2+})/Al^{3+}$ ratio in the solids to be 2.890 ± 0.119. Analyses of hydroxide and chloride are quite constant throughout the whole range of iron mole fractions in solids from 0.00 to 0.13 as well as for hydrotalcite phases synthesized at different temperatures. It was found that each formula unit contains 8.324 ± 0.361 OH^- and 0.795 ± 0.268 Cl^-. In addition, we observed that washed solids contained only traces of Na (about 1 wt. %), which means that the stoichiometric coefficient of sodium in synthesized solids was less than $Na_{0.001}$.

Measured concentrations of dissolved Mg and Al in experiments at 25 °C vary over the range from 29.50 to 666.00 μmol/kg, and from 1.11 to 435.02 μmol/kg. We observed that molalities of dissolved Al increase with the growth of iron mole fraction in solids (Table 1). The molalities of dissolved iron in these experiments were below the detection limit of ICP-OES method (0.54 μmol/kg). Therefore, for further modeling calculations and in order to determine chemical potentials of aqueous Fe^{2+} species using GEM-Selektor software, the total dissolved molalities of iron in these experiments were assumed to be equal 0.54 μmol/kg. Chemical analyses of dissolved chloride and sodium demonstrated that Cl^- and Na concentrations are constant (99.85–111.70 mmol/kg and 89.23–98.02 mmol/kg, respectively). Results of hydrotalcite syntheses at higher temperatures demonstrated that concentrations of dissolved magnesium decrease (from 666.000 to 21.5 μmol/kg) with the growth of temperature (from 25 to 60 °C) (see Table 2). At the same time Al concentrations (1.11–3.03 μmol/kg) do not depend on temperature. Measured concentrations of chloride and sodium were determined on the level 92.23–122.42 mmol/kg and 90.16–100.25 mmol/kg, respectively. In conclusion we see that the ionic strength (~ 0.1 M) of all "synthesis solutions" is generally defined by sodium content and this fact permitted the use of the Davies model for estimating activities and chemical potentials of relevant dissolved components (*i.e.*, Mg^{2+}, Fe^{2+}, Al^{3+}, OH^-, Cl^-).

4.2 Characterization of hydrotalcite-pyroaurite solids by PXRD, IR spectroscopy, TGA analyses, SEM and EDX techniques

The PXRD technique was applied in order to prove that all precipitates are indeed pure hydrotalcite-pyroaurite phases and to check that hydrotalcite-pyroaurite compositions form a continuous solid solution series. We observed that precipitates with mole fractions of iron $x\text{Fe}_{solid} = Fe^{2+}/(Fe^{2+} + Mg^{2+})$ varying from 0.00 to 0.13 display diffraction patterns (Fig. 1) typical for pure hydrotalcite-like phases [26].

This means that the amounts of any conceivable crystalline impurities in the solids (such as, gibbsite, brucite and ferric oxides and hydroxides) do not exceed the detection limit of the PXRD technique (about 1–5 wt. %) [27]. However, in precipitates with higher mole fraction of iron ($x\text{Fe}_{solid} > 0.13$), we detected additional reflexes which were attributed to lepidocrocite [28], ferric hydrates [29] or goethite [30]. The presence of these substances can be explained by the partial oxidation of Fe(II) to Fe(III) during the preparation of samples. This is confirmed by numerous observations of very fast iron oxidation processes in similar Fe(II)- containing phases (called as "green rusts"), when in contact with air or another oxidizing agent green rust phases transform into magnetite, goethite α-FeOOH, lepidocrocite γ-FeOOH, akaganeite, or ferrihydrite $5Fe_2O_3 \cdot 9H_2O$ [31–35]. It was concluded that the application of a glove-box with an argon atmosphere would allow us to exclude the oxidation of Fe(II) in the synthesized hydrotalcite-pyroaurite compositions. Unit-cell parameters of hydrotalcite-pyroaurite phases with $x\text{Fe}_{solid}$ from 0.00 to 0.13 have been calculated using a Bragg-type evaluation according to the scheme described previously [20]. Evaluated unit-cell parameters $a_o = b_o$ and c_o (Table 5, Figs. 2 and 3) of hydrotalcite-pyroaurite solids synthesized at 25 °C are represented as a function of mole fraction of iron.

As seen on Fig. 2, the unit-cell parameter $a_o = b_o$ correlates with the mole fraction of iron and was approximated by using the linear function (see dashed line in Fig. 2). More-
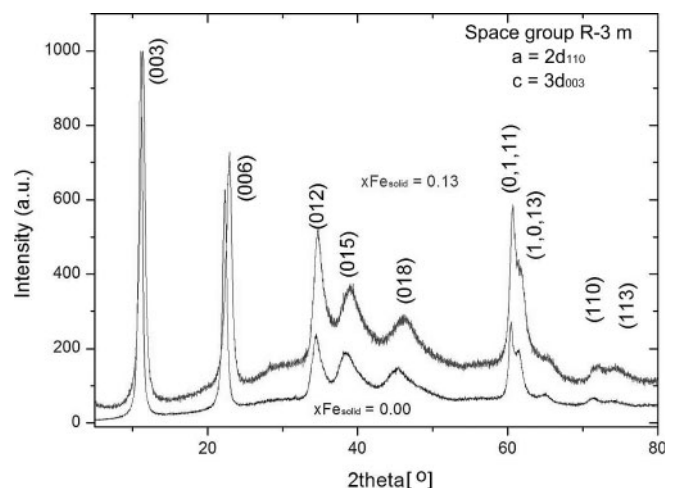
Fig. 1. X-ray diffractograms of synthetic hydrotalcite-pyroaurite solids with $x\text{Fe}_{solid} = 0.00$ and 0.13.

Table 5. Unit-cell parameters of synthesized hydrotalcite-pyroaurite solids synthesized at 25 °C (the present study) and at 70 °C (Curtius *et al.*, unpublished data) determined from Bragg evaluation and refined in the space group *R-3 m*.

| Approximate mole fraction of iron solid	$a_o = b_o$ (Å)	c_o (Å)	Source
0.000	3.082 ± 0.002	24.065 ± 0.010	(1)
0.000	3.066 ± 0.001	23.959 ± 0.006	(2)
0.033	3.061 ± 0.002	23.783 ± 0.010	(1)
0.033	3.067 ± 0.001	23.951 ± 0.006	(2)
0.033	3.065 ± 0.001	23.779 ± 0.006	(2)
0.067	3.051 ± 0.002	23.591 ± 0.010	(1)
0.067	3.062 ± 0.001	23.612 ± 0.006	(2)
0.100	3.063 ± 0.002	23.351 ± 0.010	(1)
0.133	3.063 ± 0.002	23.286 ± 0.010	(1)
0.167	3.042 ± 0.001	23.011 ± 0.006	(2)
0.167	3.057 ± 0.001	23.243 ± 0.006	(2)

References: (1) – the present study, (2) – Curtius *et al.*, unpublished data.
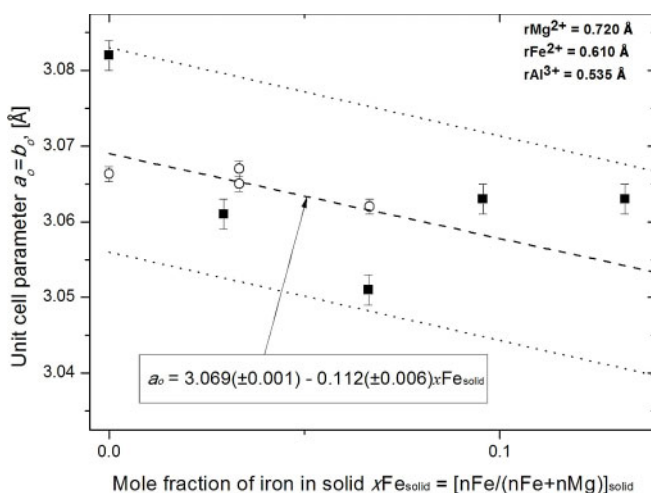
Fig. 2. Unit cell parameters $a_o = b_o$ as a function of the mole fraction of iron. The dashed line represents the linear approximation of experimental points. The dotted lines correspond to the theoretical curves based on a regular octahedral layer. Filled squares represent parameters determined from samples synthesized at 25 °C, open circles demonstrate unit cell parameters of solids synthesized at 70 °C (Curtius *et al.*, unpublished data).

over, we found that the theoretical dependence (see dotted curves) of unit-cell distance $a_o = b_o$ on the mole fractions of iron for an idealized octahedral layer (where ionic radii are $r_{Mg^{2+}} = 0.720$ Å, $r_{Fe^{2+}} = 0.610$ Å, $r_{Al^{3+}} = 0.535$ Å [36]) has the same slope as the linear approximation. This can be explained by the fact that hydrotalcite-pyroaurite solids in the range $x\text{Fe}_{solid}$ from 0.00 to 0.13 form continuous solid solution series and the variation of cell-parameter $a_o = b_o$ is in agreement with the Vegard's law [37].

On the other hand, the lattice parameter c_o corresponds to three layer rhombohedral polytype 3R and is represented as a function of iron mole fraction shown in Fig. 3.

As seen on this plot, this unit-cell parameter c_o does not change significantly with increasing mole fraction of iron. The slight decrease (from 24.065 to 23.011 Å) can be attributed to the isostructural substitution of Mg^{2+} (0.720 Å) by smaller Fe^{2+} (0.610 Å).
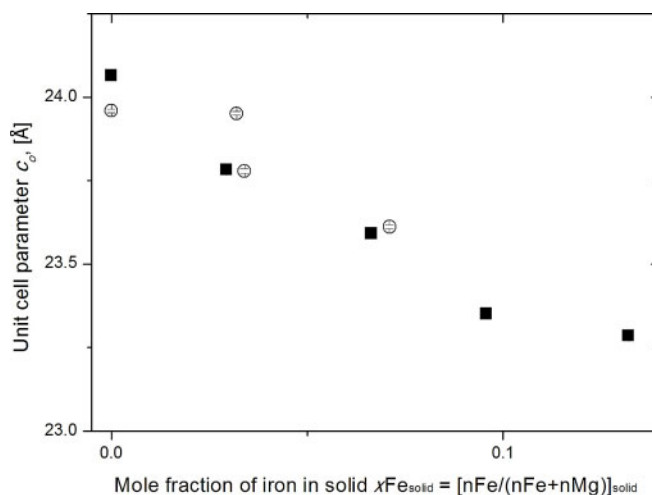
Fig. 3. Dependence of the unit cell parameter c_o on the mole fraction of Fe. Filled squares demonstrate results from samples synthesized at 25 °C, open circles represent unit cell parameters of solids synthesized at 70 °C (Curtius *et al.*, unpublished data).

Table 6. Unit-cell parameters of hydrotalcite solids synthesized at 25, 40, 45, 50, 55 and 60 °C and determined from Bragg evaluation and refined in the space group *R-3 m*.

(Mg^{2+}/Al^{3+}) ratio in solid	Temperature (°C)	$a_o = b_o$ (Å)	c_o (Å)
2.912	25	3.082 ± 0.002	24.065 ± 0.010
2.765	25	3.065 ± 0.002	23.863 ± 0.010
2.950	40	3.086 ± 0.002	23.778 ± 0.010
2.901	45	3.099 ± 0.002	23.784 ± 0.010
2.863	50	3.090 ± 0.002	23.641 ± 0.010
2.879	55	3.071 ± 0.002	23.860 ± 0.010
2.865	60	3.100 ± 0.002	23.644 ± 0.010

Unit-cell parameters of synthesized pure hydrotalcite ($x\text{Fe}_{solid} = 0$) solids as a function of temperature of co-precipitation experiments are represented in Table 6. We observed that the measured unit-cell parameters $a_o = b_o$ and c_o are remarkably constant (3.085 ± 0.013 Å and 23.805 ± 0.146 Å, respectively) in all synthesized hydrotalcites and do not deviate significantly with increasing temperature. The correlation between cationic (Mg^{2+}/Al^{3+}) ratios in hydrotalcite solids and lattice parameters also was not observed. However, due to the difference of ionic radii of Mg^{2+} (0.720 Å) and Al^{3+} (0.535 Å) the increase of cationic (Mg^{2+}/Al^{3+}) ratio should increase the intermetallic distances (*i.e.*, $a_o = b_o$ parameters) in the hydrotalcite structure.
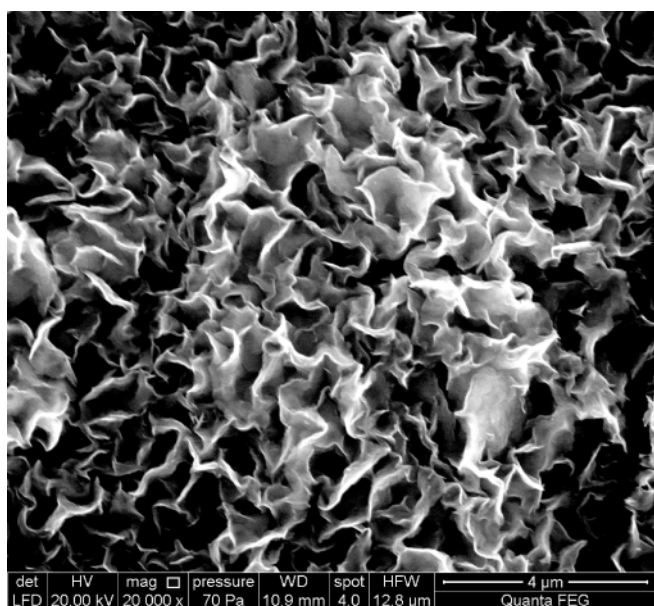
Infrared spectroscopic measurements have been performed to identify the nature of interlayer anions and to investigate its interaction with brucite-like layers. We found that IR spectra show very strong hydroxyl- and water-stretching bands at 3450 cm⁻¹ and 1640 cm⁻¹, respectively. Other strong bands at about 850 cm⁻¹, were attributed to the translational movements of the oxygen in the octahedral brucite-like layers. The quite weak band due to adsorbed carbonate was detected at 1370 cm⁻¹. The presence of carbonate in precipitates is explained by the very strong affinity of LDHs for this anion. We expect that carbonate was adsorbed during the preparation of the samples for IR analyses when LDH powders were mixed with KBr phase or even during the synthesis procedure.
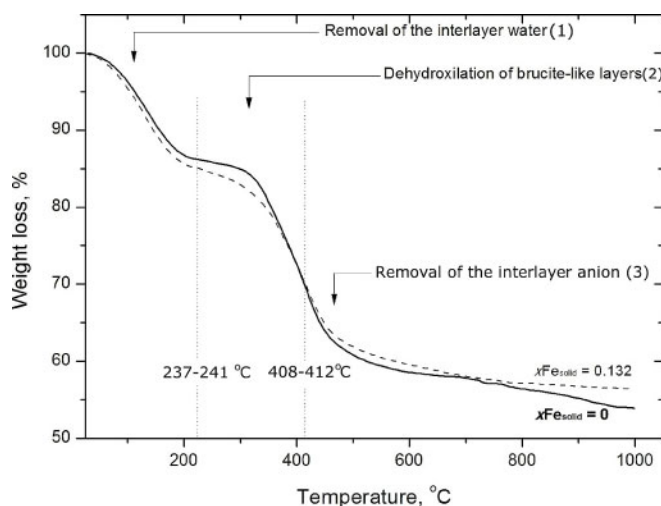
Fig. 4. TGA curves of solids with $x\text{Fe}_{\text{solid}} = 0.00$ (solid curve) and with $x\text{Fe}_{\text{solid}} = 0.132$ (dashed curve). The applied heating rate was 10 °C/min. Decomposition steps are shown according to (Rives, 2002).

Thermogravimetric analyses together with coupled differential scanning calorimetric measurements of synthesized hydrotalcite-pyroaurite series with mole fraction of iron from 0.00 to 0.13 demonstrated that thermal decomposition includes three main stages (Fig. 4).

These results are in agreement with the previous literature data [38–40] showing that thermal decomposition of layered double hydroxides takes place in three steps: (1) the removal of the interlayer water, (2) the decomposition of structural hydroxyl groups and finally (3) the loss of the interlayer anions. For the current compounds, these three decomposition steps were evaluated by determining the second derivative TGA-curve and confirmed by the results of DSC measurements. We demonstrated that: (1) the first endothermic peaks occur between room temperature and approximately 239 °C, with its maxima at 136 °C due to desorption of the interlayer water; (2) the second endothermic peaks between 239 °C and 410 °C indicate a partial dehy-

droxylation of brucite-like layer. The final (3) decomposition step from 410 °C to 1000 °C is recognized as loss of interlayer anions and formation of the mixture of Mg, Al and Fe oxides. We found that the incorporation of divalent iron into the structure of solids does not strongly affect their thermal stability because we observed that an increase of the mole fraction of iron does not cause a significant effect on the temperatures of removal interlayer water, dehydroxylation and removal of interlayer anions.

Scanning electron microphotographs demonstrated that majority of precipitated samples were typical for LDHs "sand rose" aggregates [41] (Fig. 5). The most common morphologies of the particles were based on deformed hexagonal platelets, 1–20 μm in size.
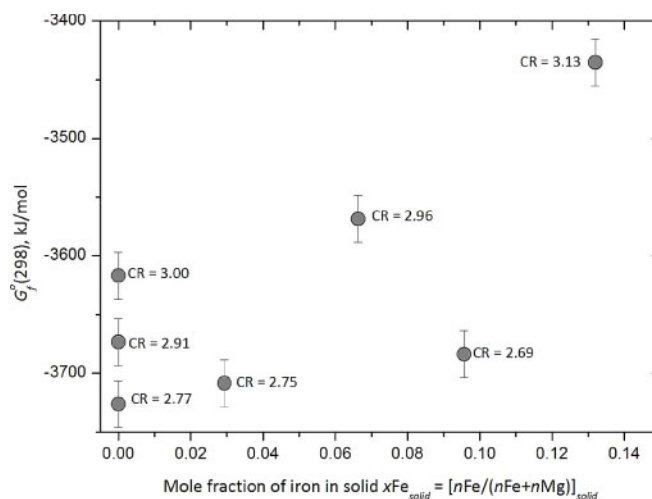
Using energy dispersive X-ray analyses of individual particles we investigated the elemental distribution and these results showed that in synthesized phases with $x\text{Fe}_{\text{solid}}$ from 0 to 0.13 the distribution of Mg, Al, Fe, C, O and Cl components is generally homogeneous and no other phases were observed.

4.3 Estimation of molar Gibbs free energies and standard entropies of hydrotalcite-pyroaurite solids

The solids as described in Tables 3 and 4 precipitated from the solutions presented in Tables 1 and 2, respectively. In this study we neglected the possible effect of oversaturation and we assumed equilibrium between the precipitated solids and their corresponding "synthesis solutions". This allowed the calculation of the molar Gibbs free energies of precipitates by modeling compositions of liquids and calculating chemical potentials of relevant dissolved compounds using GEM-Selektor [22] as described in Sect. 3.1.
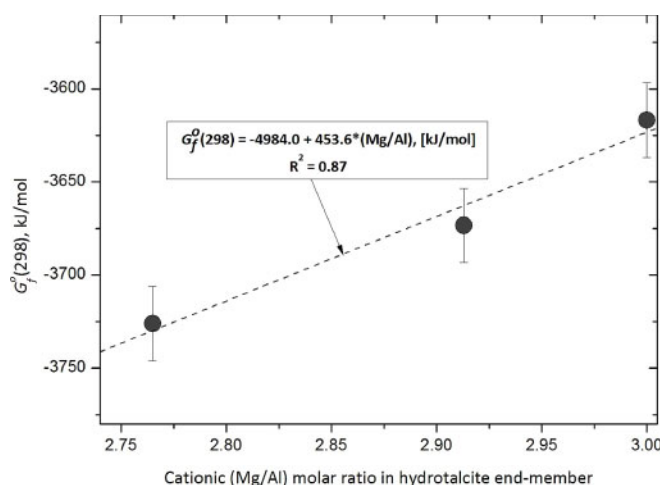
The estimated standard Gibbs free energies of hydrotalcite-pyroaurite phases as a function of iron mole fraction $x\text{Fe}_{\text{solid}} = n\text{Fe}/(n\text{Fe} + n\text{Mg})$ are demonstrated in Fig. 6. As seen in Fig. 6, there is a tendency of $G_{\text{f}}^{\circ}(298)$ growth when the mole fraction in synthesized solids increases.

However, this dependence is not clear and in order to improve the situation we examined the dependence of molar

Fig. 5. Typical morphology of the Mg-Al-Fe-LDH precipitate ($x\text{Fe}_{\text{solid}} = 0.132$), investigated by SEM.

Fig. 6. Standard Gibbs free energies of "water-free" solids calculated as a function of the mole fraction of iron.
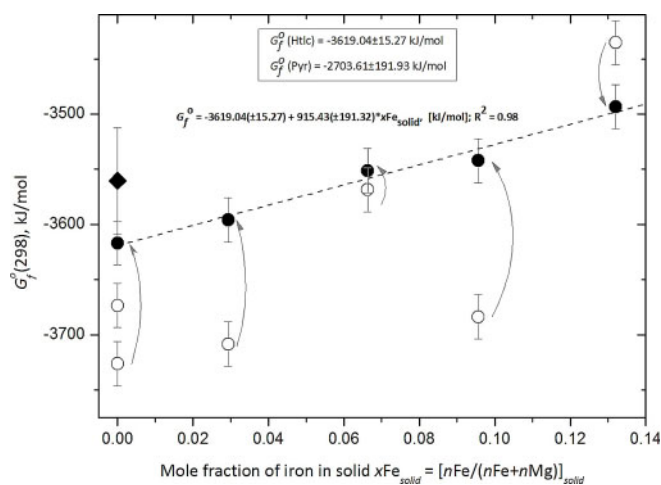
Fig. 7. Standard Gibbs free energies of "water-free" hydrotalcite solids represented as a function of Mg/Al molar ratio.

Gibbs free energy on the Mg/Al molar ratio in synthesized hydrotalcite phases (Fig. 7).

As seen on this plot, standard Gibbs free energies of hydrotalcite ($x\mathrm{Fe}_{solid} = 0$) can be represented as a linear function of the measured Mg/Al cationic ratio. This linear dependence allowed us to extrapolate compositions of synthesized iron-containing compositions to the idealized $(\mathrm{Mg} + \mathrm{Fe})/\mathrm{Al} = 3/1$ stoichiometry and to obtain significantly improved linear relationship: $G_f^\circ = (-3619.04 \pm 15.27) + (915.43 \pm 191.32) \cdot x\mathrm{Fe}_{solid}$ (kJ/mol), $R^2 = 0.98$ (Fig. 8), from which we determined the standard Gibbs free energies of end-members: $G_f^\circ(\mathrm{Htlc}) = -3619.04 \pm 15.27$ kJ/mol; $G_f^\circ(\mathrm{Pyr}) = -2703.61 \pm 191.93$ kJ/mol.

This is in agreement with the G_f° value for hydrotalcite from the study of Bravo-Suárez [42]. These authors determined a value of -890.10 ± 12.06 kJ/mol for a "water-free" solid having the stoichiometry $[\mathrm{Mg}_{0.75}\mathrm{Al}_{0.25}(\mathrm{OH})_2](\mathrm{Cl}_{0.25})$. Normalizing this stoichiometry to three Mg (*i.e.*, $\mathrm{Mg}_3\mathrm{Al}_1(\mathrm{OH})_8\mathrm{Cl}_1$) gives -3560.40 ± 48.25 kJ/mol. In order
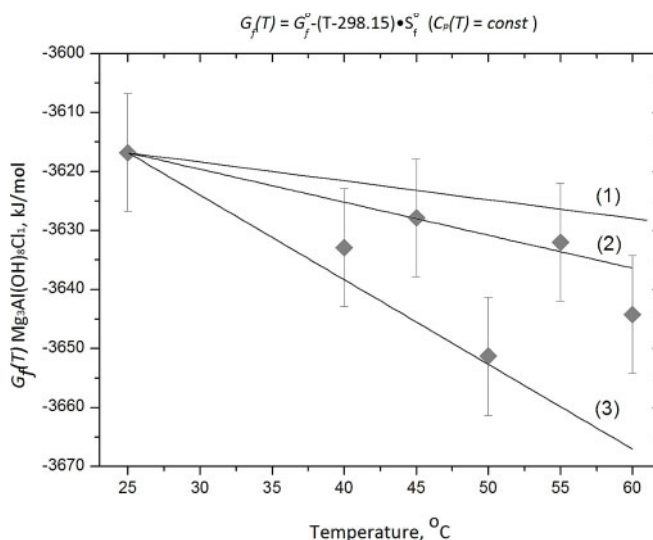
to assess the influence of the intercalated anions on the aqueous solubility of hydrotalcite-like solids we compared the standard Gibbs free energy of Cl-bearing hydrotalcite (-3619.04 ± 15.27 kJ/mol) obtained in the present study with data presented for CO_3-containing hydrotalcite (-3746.90 ± 11.00 kJ/mol) [19]. The difference 127.86 ± 18.82 kJ/mol denotes the effect of the intercalated anion on the aqueous solubility, demonstrating that Cl^--containing hydrotalcite have to be more soluble than the carbonate-bearing hydrotalcite. This conclusion confirms recent literature results of Allada *et al.*, [8]. Based on calorimetric measurements these authors predicted equilibrium constants for the dissolution of Cl^- and CO_3^{2-}-containing hydrotalcites and concluded that carbonate substances will be less soluble than solids bearing chloride anion.

To provide reasonable temperature and pressure corrections for the thermodynamic properties of the hydrotalcite end-member, we estimated the absolute molar entropy at 298 K and 1 bar. This has been done using the method of Helgeson and using results of hydrotalcite syntheses at variable (25, 40, 45, 50, 55 and 60 °C) temperatures (see Sect. 3.2).

Applying the method of Helgeson we found that absolute entropy of hydrotalcite composition is equal to 318.40 J/mol K. On the other hand, the second approach demonstrated that absolute entropy varies in the range from 558.93 to 1434.75 J/mol K.

These significant discrepancies in estimates of standard molar entropy are demonstrated on the temperature dependence of Gibbs free energies of hydrotalcite end-member (Fig. 9).

Assuming that heat capacity of hydrotalcite is a constant over the temperature from 25 to 60 °C, we were able to construct the theoretical dependence of Gibbs free energy on the

Fig. 8. Standard Gibbs free energies of hydrotalcite-pyroaurite solids calculated as mole fraction of iron. Open circles are calculated from actually analyzed stoichiometries of synthesized solids. Filled circles are results obtained from idealized $(\mathrm{Mg}_{1-x}, \mathrm{Fe}_x)_3\mathrm{Al}_1$ stoichiometries of hydrotalcite-pyroaurite solids (see text above). The diamond symbol represents a result from Bravo-Suárez *et al.*, 2004 normalized to Mg_3-stoichiometry.

Fig. 9. Gibbs free energy of hydrotalcite end-member as a function of temperature. Diamond symbols correspond to results from coprecipitation experiments at different temperatures and using the idealized $\mathrm{Mg}_3\mathrm{Al}_1$-stoichiometry. Lines (1), (2), (3) show results obtained from temperature dependences of Gibbs free energies corresponding to Eq. (8) with absolute molar entropies are equal to 318.40, 558.93, 1434.75 J/mol K, respectively.

temperature from the following relation:

$$G_f(T) = G_f^\circ - (T - 298.15) \cdot S_f^\circ \qquad (8)$$

From Fig. 9 it can be seen that all estimates of absolute molar entropies do not fit experimental results sufficiently well. For the possible further work in order to provide more accurate information about absolute molar entropies, we would recommend to perform calorimetric measurements. The providing data about absolute molar entropy of hydrotalcite solids by calorimetric measurements is the objective of our forthcoming separate study.

5. Discussion and conclusions

The aim of the present work was to investigate aqueous solubilities of the hydrotalcite-pyroaurite solids by using results of syntheses (by co-precipitation) experiments carried out at ambient conditions (25 °C, $P = 1$ bar) and at elevated temperatures (40, 45, 50, 55 and 60 °C). Hydrotalcite-pyroaurite solids with different iron mole fractions $x\text{Fe}_{solid} = \text{Fe}^{2+}/(\text{Mg}^{2+} + \text{Fe}^{2+})$ varying from 0 to 0.13 have been successfully synthesized. The $(\text{Mg}^{2+} + \text{Fe}^{2+})/\text{Al}^{3+}$ ratios of these precipitates were kept constant at 2.890 ± 0.119. All PXRD patterns of these solids indicated the formation of a single phase belonging to the hydrotalcite-pyroaurite solid solution series [26]. However, products of syntheses with iron mole fraction higher than 0.13 display additional PXRD reflexes attributed to the mixture of Fe oxides and hydroxides (for instance, lepidocrocite, ferric hydrates or goethite) [28–30]. Formation of these phases was explained by very fast oxidation of hydrotalcite-pyroaurite solids in contact with air or other oxidizing agent during the preparation (or during PXRD measurements) of samples.

The thermal behavior of samples with $0 \le x\text{Fe}_{solid} \le 0.13$ is that expected for LDH with 3 main decomposition steps (removal of interlayer water, dehydroxylation of brucite-like layers and removal of interlayer anion). Temperatures of these three events do not depend on the content of iron in solids. TGA-DSC measurements were used here successfully for measuring the water, hydroxyl and chloride-content. For hydrotalcite-like phases this is usually difficult to achieve because the three decomposition steps are often not well separated.

Infrared spectra of synthesized solids show strong hydroxyl- and water-stretching bands at 3450 cm^{-1} and 1640 cm^{-1}, respectively. The strong bands at about 850 cm^{-1} have been attributed to the translational movements of the oxygen in the octahedral brucite-like layers. The quite weak band at 1370 cm^{-1} was attributed to adsorbed traces of carbonate ions. We explained the presence of carbonate in precipitates by very strong affinity of hydrotalcite-like solids to this anion.

An extended aim of the present study included quantifying the standard Gibbs free energies and absolute molar entropies of hydrotalcite-pyroaurite compositions. These aims can be achieved by analyzing solution- and solid compositions and assuming that thermodynamic equilibrium between precipitated solid and mother solution was reached. All chemical analyses have been performed by

using ICP-OES, photometric, EDX and TGA techniques and the results of thermodynamic calculations are described in Sect. 4.3.

We demonstrated that the estimated values of standard Gibbs free energies correlate strongly with the stoichiometry of hydrotalcite-pyroaurite solids. Firstly, we observed that values of molar Gibbs free energies are related with Me^{2+}/Me^{3+} cationic ratio. In fact, the growth of Mg^{2+}/Al^{3+} ratio from 2.77 to 3.00 in hydrotalcite end-member results in increase of Gibbs free energy value from -3673.37 to -3619.04 kJ/mol. This observation permitted to normalize all estimates of G_f° with respect to idealized hydrotalcite-pyroaurite compositions with cationic ratio $(\text{Mg}^{2+} + \text{Fe}^{2+})/\text{Al}^{3+} = 3 : 1$ and $0 < x\text{Fe}_{solid} \le 0.13$. As a result, we observed that the estimates of standard Gibbs free energy follows the linear function of iron mole fraction and, therefore, yields the following first estimates: -3619.04 ± 15.27 and -2703.61 ± 191.93 kJ/mol for Htlc and Pyr end-members, respectively.

Applying Helgeson's method [25] and results of hydrotalcite syntheses at elevated (40, 45 50, 55 and 60 °C) temperatures we obtained absolute molar entropy estimates for hydrotalcite end-member. It was recognized that two approaches do not fit experimental results sufficiently well and these clearly seems the need to perform more precise calorimetric measurements. Particularly, it is expected that such a method will be appropriate for a more detailed comparison of stability properties of CO$_3^{2-}$- and Cl$^-$ bearing LDHs and, finally, for specifying the effect of intercalated anion on the aqueous solubilities of hydrotalcite-like solids. At the present state of the investigation we were not able to perform thermodynamic and solubility modeling of hydrotalcite-pyroaurite system from point of view of solid solution concept due to the missing information about: 1) the existence of hydrotalcite-pyroaurite phases with $x\text{Fe}_{solid} > 0.13$ and, especially, pyroaurite end-member, and 2) the degree of oversaturation in "synthesis solutions". Because of this, we believe that further co-precipitation experiments as well as dissolution studies with synthesized solids will provide more results, extending the knowledge about the behavior of hydrotalcite-pyroaurite system in aqueous environment, *i.e.*, particularly, at conditions of nuclear waste repositories.

References

1. Aramendia, M. A., Borau, V., Jimenez, U., Marinas, J. M., Ruiz Jr., Urbano, F. J.: Comparative study of Mg/M(III) (M = Al, Ga, In) layered double hydroxides obtained by co-precipitation and the sol-gel method. J. Solid State Chem. **168**(1), 156–161 (2002).
2. Boclair, J. W., Braterman, P. S., Jiang, J. P., Lou, S. W., Yarberry, F.: Layered double hydroxide stability. 2. Formation of Cr(III)-containing layered double hydroxides directly from solution. Chem. Mater. **11**(2), 303–307 (1999).
3. Carteret, C., Gregoire, B., Ruby, C.: Tunable composition of Ni(II)-Al(III) and Ni(II)-Fe(III) layered hydroxides within a wide range of layer charge. Solid State Sc. **13**(1), 146–150 (2011).

4. Curtius, H., Ufer, K., Dardenne, K.: Preparation and characterization of Zr-IV-containing Mg-Al-Cl layered double hydroxide. Radiochim. Acta **97**(8), 423–428 (2009).

5. Rousselot, I., Taviot-Gueho, C., Leroux, F., Leone, P., Palvadeau, P., Besse, J. P.: Insights on the structural chemistry of hydrocalumite and hydrotalcite-like materials: Investigation of the series $Ca_2M^{3+}(OH)_6Cl\cdot2H_2O$ (M^{3+}: Al^{3+}, Ga^{3+}, Fe^{3+}, and Sc^{3+}) by X-ray powder diffraction. J. Solid State Chem. **167**(1), 137–144 (2002).

6. Ulibarri, M. A., Cornejo, J., Hernandez, M. J.: Effects of hydrothermal treatment on textural properties of $[Al_2Li(OH)_6]_2CO_3\cdot nH_2O$. J. Mater. Sci. **22**(4), 1168–1172 (1987).

7. Wang, J. D., Serrette, G., Tian, Y., Clearfield, A.: Synthetic and catalytic studies of inorganically pillared and organically pillared layered double hydroxides. Appl. Clay Sci. **10**(1–2), 103–115 (1995).

8. Allada, R. K., Pless, J. D., Nenoff, T. M., Navrotsky, A.: Thermochemistry of hydrotalcite-like phases intercalated with CO_3^{2-}, NO_3^-, Cl^-, I^-, and ReO_4^-. Chem. Mater. **17**(9), 2455–2459 (2005).

9. Brindley, G. W., Kikkawa, S.: Thermal-behavior of hydrotalcite and of anion-exchanged forms of hydrotalcite. Clays Clay Mineral. **28**(2), 87–91 (1980).

10. Carlino, S.: The intercalation of carboxylic acids into layered double hydroxides: A critical evaluation and review of the different methods. Solid State Ion. **98**(1–2), 73–84 (1997).

11. Carrado, K. A., Kostapapas, A., Suib, S. L.: Layered double hydroxides (LDHs). Solid State Ion. **26**(2), 77–86 (1988).

12. Chibwe, K., Jones, W.: Intercalation of organic and inorganic anions into layered double hydroxides. J. Chem. Soc.-Chem. Commun. **(14)**, 926–927 (1989).

13. Chisem, I. C., Jones, W.: Ion-exchange properties of lithium aluminum layered double hydroxides. J. Mater. Chem. **4**(11), 1737–1744 (1994).

14. Miyata, S., Kumura, T.: Synthesis of new hydrotalcite-like compounds and their physicochemical properties. Chem. Lett. **8**, 843–848 (1973).

15. Newman, S. P., Jones, W.: Synthesis, characterization and applications of layered double hydroxides containing organic guests. New J. Chem. **22**(6), 649 (1998).

16. NAGRA TECHNICAL REPORT 02-05: Project Opalinus Clay. Demonstration of disposal feasibility for spent fuel, vitrified high-level waste and long-lived intermediate-level waste (Entsorgungsnachweis), NAGRA: Wettingen 2002.

17. Allada, R. K., Navrotsky, A., Berbeco, H. T., Casey, W. H.: Thermochemistry and aqueous solubilities of hydrotalcite-like solids. Science **296**(5568), 721–723 (2002).

18. Johnson, C. A., Glasser, F. P.: Hydrotalcite-like minerals $(M_2Al(OH)_6(CO_3)_{0.5}\cdot xH_2O$, where M = Mg, Zn, Co, Ni) in the environment: synthesis, characterization and thermodynamic stability. Clays Clay Mineral. **51**(1), 1–8 (2003).

19. Rozov, K., Berner, U., Kulik, D., Diamond, L. W.: Solubility and thermodynamic properties of carbonate-bearing hydrotalcite-pyroaurite solid solutions with 3 : 1 Mg/(Al + Fe) mole ratio. Clays Clay Mineral. **59**(3), 215–232 (2011).

20. Rozov, K., Berner, U., Taviot-Gueho, C., Leroux, F., Renaudin, G., Kulik, D, Diamond, L. W. : Synthesis and characterization of the LDH hydrotalcite-pyroaurite solid-solution series. Cement Concrete Res. **40**(8), 1248–1254 (2010).

21. Mazeina, L., Curtius, H., Fachinger, J., Odoj, R.: Characterization of secondary products of uranium-aluminum material test reactor fuel element corrosion in repository-relevant brine. J. Nucl. Mater. **323**(1), 1–7 (2003).

22. Kulik, D., GEM-Selektor. Research package for thermodynamic modeling of aquatic (geo)chemical systems by Gibbs Energy Minimization (GEM). http://gems.web.psi.ch.

23. Hummel, W., Berner, U., Curti, E., Pearson, F. J., Thoenen, T.: Nagra/PSI chemical thermodynamic data base 01/01. Radiochim. Acta **90**(9–11), 805–813 (2002).

24. Shock, E. L., Sassani, D. C., Willis, M., Sverjensky, D. A.: Inorganic species in geologic fluids: Correlations among standard molar thermodynamic properties of aqueous ions and hydroxide complexes. Geochim. Cosmochim. Acta **61**(5), 907–950 (1997).

25. Helgeson, H. C., Delany, J. M., Nesbitt, H. W., Bird, D. K.: Summary and critique of the thermodynamic properties of rock-forming minerals. Am. J. Sci. **278**, 1–229 (1978).

26. Malherbe, F., Besse, J. P.: Investigating the effects of guest-host interactions on the properties of anion-exchanged Mg-Al hydrotalcites. J. Solid State Chem. **155**(2), 332–341 (2000).

27. Lanfranco, A. M., Schofield, P. F., Murphy, P. J., Hodson, M. E., Mosselmans, J. F. W., Valsami-Jones, E.: Characterization and identification of mixed-metal phosphates in soils: the application, of Raman spectroscopy. Mineral. Mag. **67**(6), 1299–1316 (2003).

28. Eggleton, R. A., Fitzpatrick, R. W.: New data and a revised structural model for ferrihydrite. Clays Clay Mineral. **36**(2), 111–124 (1988).

29. Chandy, K. C.: Thermal transformation of beta-ferric oxyhydroxide. Mineral. Mag. J. Mineral. Soc. **35**(272), 666 (1965).

30. Van der Giessen, A. A.: The structure of iron (III) oxide-hydrate gels. J. Inorg. Nucl. Chem. **28**(10), 2155–2159 (1966).

31. Christiansen, B. C., Balic-Zunic, T., Petit, P. O., Frandsen, C., Morup, S., Geckeis, H., Katerinopoulou, A., Stipp, S. L. S.: Composition and structure of an iron-bearing, layered double hydroxide (LDH) – Green rust sodium sulphate. Geochim. Cosmochim. Acta **74**(18), 5424–5425 (2010).

32. Genin, J. M. R., Ruby, C., Upadhyay, C.: Structure and thermodynamics of ferrous, stoichiometric and ferric oxyhydroxycarbonate green rusts; redox flexibility and fougerite mineral. Solid State Sci. **8**(11), 1330-1343 (2006).

33. Hansen, H. C. B., Borggaard, O. K., Sorensen, J.: Evaluation of the free-energy of formation of Fe(II)-Fe(III) hydroxide-sulfate (green rust) and its reduction of nitrite. Geochim. Cosmochim. Acta **58**(12), 2599–2608 (1994).

34. Refait, P., Genin, J. M. R.: The mechanisms of oxidation of ferrous hydroxychloride β-$Fe_2(OH)_3Cl$ in aqueous solution: the formation of akaganeite *vs*. goethite. Corros. Sci. **39**(3), 539–553 (1997).

35. Schwertmann, U., Fechter, H.: The formation of green rust and its transformation to lepidocrocite. Clay Miner, **29**(1), 87–92 (1994).

36. Shannon, R. D.: Revised effective ionic-radii and systematic studies of interatomic distances in halides and chalcogenides. Acta Cryst. A **32**, 751–767 (1976).

37. Danton, A. R., Ashcroft, N. W.: Vegard's law. Phys. Rev. A **13**(6), 3161–3164 (1991).

38. Miyata, S.: Physicochemical properties of synthetic hydrotalcites in relation to composition. Clays Clay Mineral. **28**(1), 50–56 (1980).

39. Frost, R. L., Vagvolgyi, V., Palmer, S. J., Kristof, J., Horvath, E.: Mechanism for hydrotalcite decomposition: A controlled rate thermal analysis study. J. Colloid Interf. Sci. **318**(2), 302–308 (2008).

40. Rives, V.: Characterization of layered double hydroxides and their decomposition products. Mater. Chem. Phys. **75**(1–3), 19–25 (2002).

41. Mistra, C., Perrota, J.: Composition and properties of synthetic hydrotalcites. Clays Clay Minerals **40**, 45–150 (1992).

42. Bravo-Suarez, J. J., Paez-Mozo, E. A., Oyama, S. T.: Models for the estimation of thermodynamic properties of layered double hydroxides: Application to the study of their anion exchange characteristics. Quimica Nova **27**(4), 574–581 (2004).